

AD-A096 779

AEROSPACE CORP EL SEGUNDO CA SPACE SCIENCES LAB

F/G 3/2

SOLAR FLARE X-RAY SPECTRA BETWEEN 7.8 AND 23.0 ANGSTROMS.(U)

APR 81 D L MCKENZIE, P B LANDECKER

F04701-80-C-0081

UNCLASSIFIED

TR-0081(6960-01)-2

SD-TR-81-34

NL

1-1
1-1
1-1

1

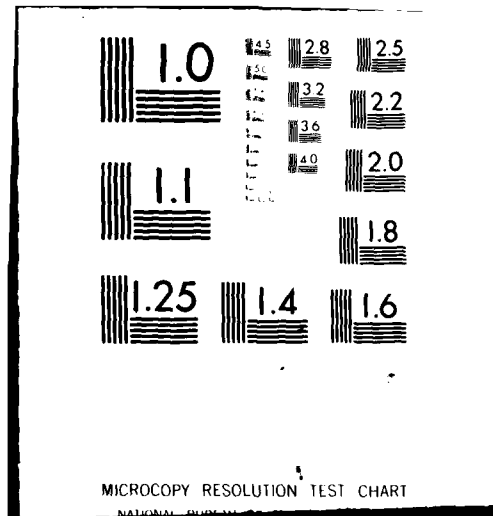
END

DATE

FILED

5-81

DTIC



LEVEL II

(12)

**Solar Flare X-Ray Spectra
Between 7.8 and 23.0 Angstroms**

D. L. MCKENZIE, P. B. LANDECKER, R. M. BROUSSARD,
H. R. RUGGE, and R. M. YOUNG
Space Sciences Laboratory
Laboratory Operations
The Aerospace Corporation
El Segundo, Calif. 90245

U. FELDMAN and G. A. DOSCHEK
E. O. Hulbert Center for Space Research
Naval Research Laboratory
Washington, D.C. 20025

1 April 1981

DTIC
ELECTE
S MAY 12 1981 **D**
E

APPROVED FOR PUBLIC RELEASE;
DISTRIBUTION UNLIMITED

Prepared for
SPACE DIVISION
AIR FORCE SYSTEMS COMMAND
Los Angeles Air Force Station
P.O. Box 92960, Worldway Postal Center
Los Angeles, Calif. 90009

81 5 12 006

AD A098779

DTIC FILE COPY

This report was submitted by The Aerospace Corporation, El Segundo, CA 90245, under Contract No. FO4701-80-C-0081 with the Space Division, Contracts Management Office, P.O. Box 92960, Worldway Postal Center, Los Angeles, CA 90009. It was reviewed and approved for The Aerospace Corporation by G. A. Paulikas, Director, Space Sciences Laboratory. Gerhard E. Aichinger was the project officer for Mission-Oriented Investigation and Experimentation (MOIE) Programs.


This report has been reviewed by the Public Affairs Office (PAS) and is releasable to the National Technical Information Service (NTIS). At NTIS, it will be available to the general public, including foreign nations.

This technical report has been reviewed and is approved for publication. Publication of this report does not constitute Air Force approval of the report's findings or conclusions. It is published only for the exchange and stimulation of ideas.



Gerhard E. Aichinger
Project Officer

FOR THE COMMANDER


Evan R. Brossman, Chief
Contracts Management Office

UNCLASSIFIED

SECURITY CLASSIFICATION OF THIS PAGE (When Data Entered)

19 REPORT DOCUMENTATION PAGE		READ INSTRUCTIONS BEFORE COMPLETING FORM	
1. REPORT NUMBER SD-TR-81-34	2. GOVT ACCESSION NO. AD-A098	3. RECIPIENT'S CATALOG NUMBER 4179	
4. TITLE (and Subtitle) SOLAR FLARE X-RAY SPECTRA BETWEEN 7.8 AND 23.0 ANGSTROMS	5. TYPE OF REPORT & PERIOD COVERED Technical Report	6. PERFORMING ORG. REPORT NUMBER TR-0081(6960-01)-2	
7. AUTHOR(s) D. L. McKenzie, P. B. Landecker, R. M. Broussard, H. R. Rugge, R. M. Young, U. Feldman, and G. A. Doschek	8. CONTRACT OR GRANT NUMBER(s) F04701-80-C-0081	9. PERFORMING ORGANIZATION NAME AND ADDRESS The Aerospace Corporation El Segundo, Calif. 90245	10. PROGRAM ELEMENT, PROJECT, TASK AREA & WORK UNIT NUMBERS
11. CONTROLLING OFFICE NAME AND ADDRESS Space Division Air Force Systems Command Los Angeles, Calif. 90009	12. REPORT DATE 1 April 1981	13. NUMBER OF PAGES 37	
14. MONITORING AGENCY NAME & ADDRESS (if different from Controlling Office) 130	15. SECURITY CLASS. (of this report) Unclassified	15a. DECLASSIFICATION/DOWNGRADING SCHEDULE	
16. DISTRIBUTION STATEMENT (of this Report) Approved for public release; distribution unlimited			
17. DISTRIBUTION STATEMENT (of the abstract entered in Block 20, if different from Report)			
18. SUPPLEMENTARY NOTES			
19. KEY WORDS (Continue on reverse side if necessary and identify by block number) Solar Flares X-ray Spectrum Solar X-rays			
20. ABSTRACT (Continue on reverse side if necessary and identify by block number) We present high resolution x-ray spectra taken during a large solar flare on 10 June 1979. Many lines of highly ionized iron are resolved and identified for the first time in solar spectra. Lines with a wide range of excitation temperatures are found to have a similar time development during the flare's rapid rise phase. We discuss density-sensitive line ratios in Fe XXI and Fe XXII.			

DD FORM 1473
(FACSIMILE)UNCLASSIFIED 407-1-1
SECURITY CLASSIFICATION OF THIS PAGE (When Data Entered)

PREFACE

The success of the Aerospace P78-1 experiments is primarily attributable to the senior engineers responsible for the instruments: W. T. Chater, C. K. Howey, and R. L. Williams. We also wish to thank P. A. Carranza, A. DeVito, W. Eng, K. Higa, D. A. Roux, J. H. Underwood, and D. Y. Watanabe, who contributed to the design, fabrication, or testing of the payload. The support of the Air Force and Aerospace Space Test Program personnel and the Air Force Satellite Control Facility personnel is also appreciated. The satellite was built by Ball Aerospace Systems Division.

Accession For	
NTIS GRA&I	<input checked="checked" type="checkbox"/>
DTIC TAB	<input type="checkbox"/>
Unannounced	<input type="checkbox"/>
Justification	
By	
Distribution/	
Availability Codes	
Dist	Avail and/or Special
A	

CONTENTS

PREFACE.....	1
I. INTRODUCTION.....	7
II. THE FLARE.....	8
III. THE SPECTRA.....	9
REFERENCES.....	29

FIGURES

1.	Two spectra taken during the rise phase of the 1979 June 10 flare.....	10
2.	Line flux plotted as a function of time during the rise phase of the 1979 June 10 flare.....	21
3.	An enlargement of part of the upper spectrum of Figure 1 showing density sensitive Fe XXI and Fe XXII line pairs.....	25

TABLE

1.	Spectral lines.....	11
----	---------------------	----

I. INTRODUCTION

The United States Air Force Space Test Program P78-1 satellite, patterned after the NASA OSO-7 satellite, carries in its sun-pointed section a complement of solar x-ray experiments, including two collimated crystal spectrometers built by The Aerospace Corporation. Each of the spectrometers may expose either an ammonium dihydrogen phosphate (ADP; $2d = 10.64 \text{ \AA}$) crystal or a rubidium acid phthalate (RAP; $2d = 26.12 \text{ \AA}$) crystal to the mechanically collimated solar x-ray flux. The SOLEX A spectrometer (SOLEX = solar x-ray) has 20 arc sec collimation and a proportional counter detector with a $5.2 \times 10^{-3} \text{ gm/cm}^2$ beryllium entrance window, and the SOLEX B spectrometer has one arc min resolution and a channel electron multiplier array detector filtered with 1.9 \mu m of polypropylene and 245 nm of aluminum to prevent UV contamination. The crystals were stepped at the rate of 0.525 degrees/sec in 30.2 arc sec steps for the observations described in this paper. A full scan between Bragg angles of 17.4° and 61.7° ($7.8 - 23.0 \text{ \AA}$) took 84.5 seconds. The instrument and its operation are thoroughly described by Landecker, McKenzie, and Rugge (1979).

Here we present sample spectra and line identifications in the $7.8 - 23.0 \text{ \AA}$ range for the flare at N 26 W 47 on 1979 June 10 at around 0900 UT. These are the highest resolution flare spectra

in this wavelength range obtained to date, and therefore many lines are observed for the first time outside the laboratory.

II. THE FLARE

The time development of the June 10 flare was somewhat unusual. The x-ray detectors on SOLRAD 11 showed an abrupt rise in flux at about 0805 UT. The flux then remained nearly constant until 0845 UT when a second outburst occurred, eventually reaching a peak at the X2 level at about 0905 UT, and decaying slowly thereafter. The H α flare listing in Solar Geophysical Data Prompt Reports, issued in July, 1979, lists only one good candidate flare during this time. The event was reported by three observatories and was assigned 2B importance by the one with the most complete coverage. The H α flare started around 0804 UT and extended beyond 0900 UT. It occurred at around N26, W47 in McMath region 16051, the one viewed by the SOLEX spectrometers. The first SOLEX B spectrum we obtained, at 0807 UT, showed line fluxes somewhat higher than those arising from a typical active region. The presence of Fe XX emission, characteristic of plasmas at temperatures higher than those usually present in nonflaring active regions, leads us to believe that the flux enhancement early in the flare took place within our field of view. Our observations after 0845 UT show rapid line flux increases coincident with the second sharp flux increase measured by SOLRAD

11. This paper discusses the 7.8 - 23.0 Å line spectra obtained between the start of the major flare outburst at 0845 UT and the entry of the satellite into the Earth's shadow at around 0904 UT.

III. THE SPECTRA

Figure 1 shows two flare spectra. In the upper spectrum the flat tops on the strongest lines arise purely because of our choice of plotting scale. A full scale of 1000 counts per 32 msec was chosen to show the weaker lines more effectively. Raw data are plotted uncorrected for background, detector dead time, and instrument response. The spectral lines, with identifications, are listed in Table 1.

For each observed spectral line Table 1 lists the peak counting rate in counts per 32 msec, and the flux in units of 10^6 photon-cm⁻² - s⁻¹ for the 0901.7 UT spectrum. Because of the large number of blends and partial blends in the spectrum it was impossible to integrate over all of the line profiles in a consistent way. Therefore the flux computation was based on the peak counting rates. The errors inherent in this technique are discussed below. The flux was computed as follows. The peak counting rate was first corrected for dead time on the basis of 5.5 μs dead time per event. If the actual detector event rate is R s⁻¹ the measured rate, R_M , is given by

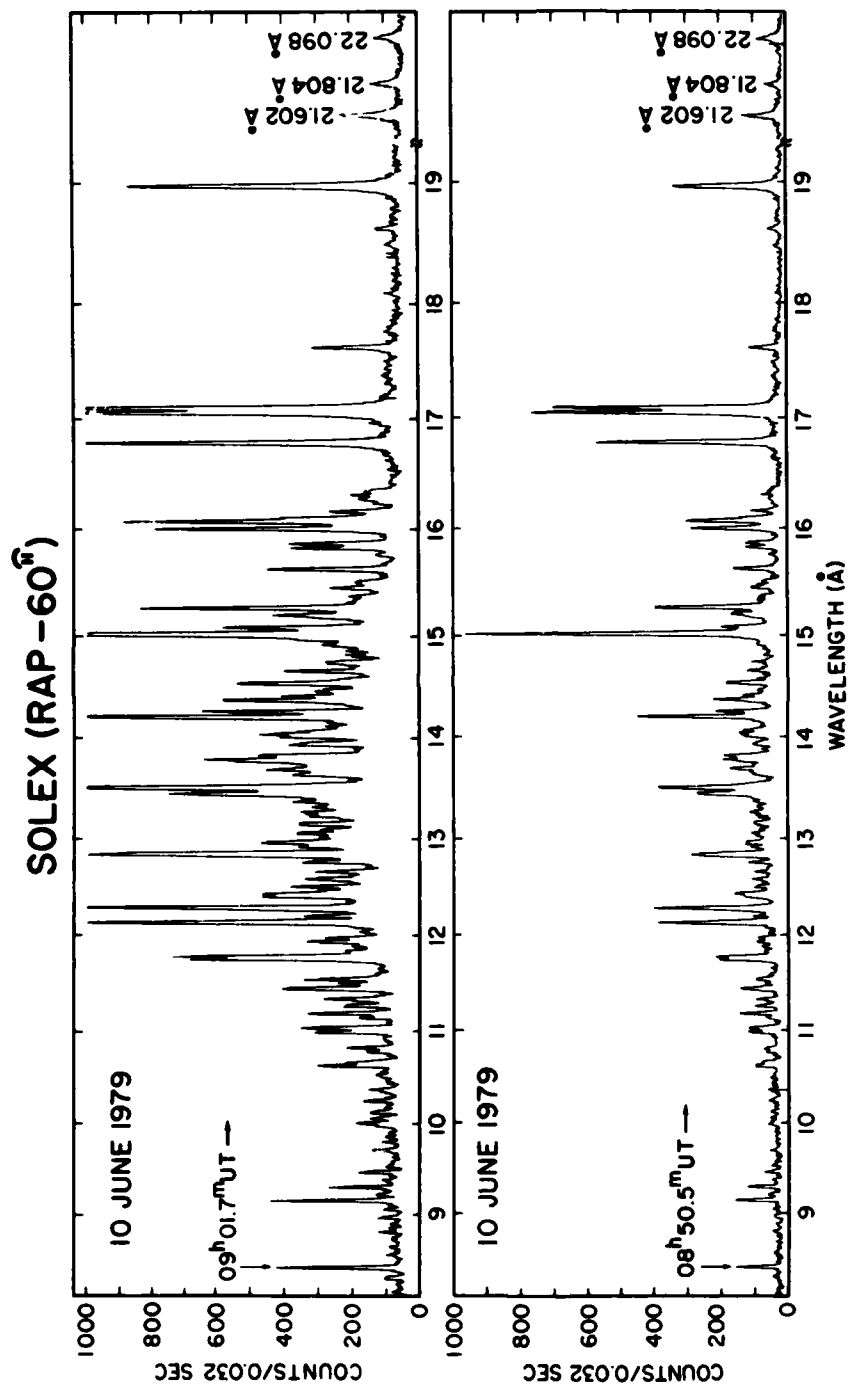


Figure 1: Two spectra taken during the rise phase of the 1979 June 10 flare. The data in Table 1 are from the upper spectrum. Note the break in the wavelength scale just above 19 Å.

TABLE 1
SPECTRAL LINES

λ_{obs} Å	$\lambda_{\text{previous}}$ Å	Ion	Transition	Peak Counts (.032s ⁻¹)	Flux (10 ⁶ cm ⁻² s ⁻¹)	Ref.
8.325	8.317	Fe XXIII	2s ² 1S ₀ - 2s4p 1P ₁	102	.033	1
	8.307	Fe XXIV	2p 2P _{3/2} - 4d 2D _{5/2}			1
8.421	8.421	Mg XII	1s 2S _{1/2} - 2p 2P _{1/2, 3/2}	434	.256	2, 3
8.823				127	.045	
8.980				129	.044	
9.073				111	.034	
9.169	9.169	Mg XI	1s 2 1S ₀ - 1s2p 1P ₁	451	.230	4
9.236	9.231	Mg XI	1s 2 1S ₀ - 1s2p 3P ₁	132	.040	5
9.319	9.314	Mg XI	1s 2 1S ₀ - 1s2s 3S ₁	276	.122	7
9.481	9.481	Ne X	1s 2S _{1/2} - 5p 2P _{1/2, 3/2}	187	.070	2
9.728	9.708	Ne X	1s 2S _{1/2} - 4p 2P _{1/2, 3/2}	147	.047	2
9.988	9.97	Ni XDK	2p 6 1S ₀ - 2p 5 4d 1P ₁			6
10.019	10.025	Na XI	1s 2S _{1/2} - 2p 2P _{1/2, 3/2}	193	.070	2
	10.102	Ni XDK	2p 6 1S ₀ - 2p 5 4d 3D ₁			6
10.136	10.120	Fe XVII	2p 6 1S ₀ - 2p 5 5p 1P ₁	151	.047	8
	10.127	Fe XVII	2p 6 1S ₀ - 2p 5 5p 3P ₁			8
10.256	10.239	Ne X	1s 2S _{1/2} - 3p 2P _{1/2, 3/2}	172	.059	2
10.382	10.386	Fe XVII	2p 6 1S ₀ - 2p 5 7d 1P ₁	156	.049	8
10.636	10.610	Fe XXIV	2s 2S _{1/2} - 3p 2P _{3/2}	308	.129	9, 10
10.664	10.653	Fe XXIV	2s 2S _{1/2} - 3p 2P _{1/2}	223	.084	9, 10
10.778	10.768	Fe XVII	2p 6 1S ₀ - 2p 5 6d 3D ₁	159	.049	6, 8
	10.765	Ne IX	1s 2 1S ₀ - 1s5p 1P ₁			11
10.791	10.80	Ni XXII	2p 3 4S - 2p 2 3d 4P	160	.051	27
10.826	10.801	Fe XIX	2p 4 3P ₂ - 2p 3 4d 3D ₃	222	.080	10
	10.979	Fe XXIII	2s 2 1S ₀ - 2s3p 1P ₁			30, 12
10.990	11.006	Na X	1s 2 1S ₀ - 1s2p 1P ₁	316	.126	2
	11.001	Ne IX	1s 2 1S ₀ - 1s4p 1P ₁			11

TABLE 1 (Con't)
SPECTRAL LINES

λ_{obs} Å	$\lambda_{\text{previous}}$ Å	Ion	Transition	Peak Counts (.032s ⁻¹)	Flux (10 ⁶ cm ⁻² s ⁻¹)	Ref.
11.031	11.018	Fe XXIII	2s ² 1S ₀ - 2s2p ³ P ₁	359	.149	12
	11.029	Fe XXIV	2p ² P _{1/2} - 3d ³ D _{3/2}			9
11.140	11.129	Fe XVII	2p ⁶ 1S ₀ - 2p ⁵ 5d ¹ P ₁	184	.058	6, 8
11.184	11.166	Fe XXIV	2p ² P _{3/2} - 3d ² D _{5/2}	337	.137	9, 10
11.255	11.250	Fe XVII	2p ⁶ 1S ₀ - 2p ⁵ 5d ³ D ₁	231	.080	6, 8
	11.253	Fe XVIII	2p ⁵ 2P _{1/2} - 2p ⁴ 4d ² D _{3/2}			14
11.269	11.262	Fe XXIV	2p ² P _{1/2} - 3s ² S _{1/2}	222	.076	13
11.336	11.318	Ni XXI	2p ⁴ 3P ₂ - 2p ³ 3d ³ D ₃	289	.111	15
	11.326	Fe XVIII	2p ⁵ 2P _{3/2} - 2p ⁴ 4d ² F _{5/2} , 2P _{3/2} , 2S _{1/2}			14, 6
11.445	11.442	Fe XXII	2s ² 2p ² P _{1/2} - 2s2p3p ² D _{3/2}			12
	11.459	Fe XXII	2s ² 2p ² P _{3/2} - 2s2p3p ² D _{5/2}	413	.178	12
	11.440	Fe XVIII	2p ⁵ 2P _{1/2} - 2p ⁴ 4d ² D _{3/2} , 2P _{1/2}			14, 6
11.497	11.421	Fe XXIV	2p ² P _{3/2} - 3s ² S _{1/2}	246	.089	10
11.537	11.526	Fe XVIII	2p ⁵ 2P _{3/2} - 2p ⁴ 4d ² D _{5/2, 3/2}	349	.142	14
11.742	11.547	Ne IX	1s ² 1S ₀ - 1s3p ¹ P ₁	689	.339	11
11.770	11.767	Fe XXII	2p ² P _{1/2} - 3d ² D _{3/2}	743	.372	9, 12
11.838	11.832	Ni XX	2p ⁵ 2P _{3/2} - 2p ⁴ (1D) 3d ² D _{5/2}	225	.045	16
11.926	11.921	Fe XXII	2p ² P _{3/2} - 3d ² D _{5/2}	341	.105	9, 12
11.971				284	.074	
12.127	12.123	Fe XVII	2p ⁶ 1S ₀ - 2p ⁵ 4d ¹ P ₁	1023	.522	25, 8
	12.134	Ne X	1s ² S _{1/2} - 2p ² P _{1/2, 3/2}			2
12.198				348	.106	

TABLE 1 (Con't)
SPECTRAL LINES

λ_{obs} Å	$\lambda_{\text{previous}}$ Å	Ion	Transition	Peak Counts (.032s ⁻¹)	Flux (10 ⁶ cm ⁻² s ⁻¹)	Ref.
12.276	12.31	Fe XXI	$2p^2\ ^3P_0 - 2p3d\ ^3D_1$	1182	.637	18
	12.263	Fe XVII	$2p^6\ ^1S_0 - 2p^54d\ ^3D_1$			25, 8
12.401	12.38	Fe XXI	$2p^2\ ^3P_2 - 2p3d\ ^3D_3$	472	.157	9
12.428	12.42	Ni XIX	$2p^6\ ^1S_0 - 2p^53d\ ^1P_1$			6, 23
12.502	12.521	Fe XVII	$2p^6\ ^1S_0 - 2p^54s\ ^1P_1$	388	.112	6, 8
12.583				345	.090	
12.657	12.641	Ni XIX	$2p^6\ ^1S_0 - 2p^53d\ ^3D_1$	314	.074	6, 23
12.755	12.76	Fe XX	$2p^3\ ^2P_{1/2} - 2p^2(^1S)3d\ ^2D_{3/2}$	354	.084	19
	12.75	Fe XX	$2p^3\ ^2D_{3/2} - 2p^2(^1D)3d\ ^2F_{5/2}$			19, 6
	12.84	Fe XX	$2p^3\ ^4S_{3/2} - 2p^2(^3P)3d\ ^4P_{5/2}$			19
12.832	12.82	Fe XX	$2p^3\ ^4S_{3/2} - 2p^2(^3P)3d\ ^4P_{3/2}$	997	.493	9, 19
	12.80	Fe XX	$2p^3\ ^4S_{3/2} - 2p^2(^3P)3d\ ^4P_{1/2}$			9, 19
12.912	12.89	Fe XX	$2p^3\ ^2D_{3/2} - 2p^2(^1D)3d\ ^2D_{5/2}$	364	.091	19
12.926				356	.087	
12.953	12.94	Fe XX	$2p^3\ ^2D_{3/2} - 2p^2(^3P)3d\ ^2D_{3/2}$	477	.132	19
12.966						
	13.015	Fe XVIII	$2s^22p^5\ ^2P_{1/2} - 2s2p^5(^1P)$ $3p\ ^2P_{1/2}$			17
13.019	13.001	Fe XVIII	$2s^22p^5\ ^2P_{1/2} - 2s2p^5(^1P)$ $3p\ ^2P_{3/2}$	303	.035	17
13.060	13.049	Fe XVIII	$2s^22p^5\ ^2P_{1/2} - 2s2p^5(^3P)$ $3p\ ^2D_{3/2}$	370	.072	17
13.089				299	.052	
13.146				363	.087	
13.166	13.159	Fe XVIII	$2s^22p^5\ ^2P_{3/2} - 2s2p^5(^3P)$ $3p\ ^2S_{1/2}$			17

TABLE 1 (Con't)
SPECTRAL LINES

λ_{obs} Å	$\lambda_{\text{previous}}$ Å	Ion	Transition	Peak Counts (.032s ⁻¹)	Flux (10 ⁶ cm ⁻² s ⁻¹)	Ref.
13.232				231	.079	
13.259		Ni XX	$2p^5 2P_{3/2} - 2p^4(^3P)$ $3s^4 P_{3/2}$			9
13.279	13.289	Fe XIX	$2p^4 3P_2 - 2p^3(^2P)3d^3 D_3$	358	.095	20
	13.319	Fe XVIII	$2s^2 2p^5 2P_{3/2} - 2s2p^5(^3P)$ $3p^4 P_{5/2}$			17
13.329	13.319	Fe XVIII	$2s^2 2p^5 2P_{3/2} - 2s2p^5(^3P)$ $3p^2 P_{1/2}$	324	.046	17
13.378	13.374	Fe XVIII	$2s^2 2p^5 2P_{3/2} - 2s2p^5(^3P)$ $3p^2 D_{5/2}$	382	.080	17
	13.451	Fe XIX	$2p^4 3P_2 - 2p^3(^2D)3d^1 F_3$			20
	13.447	Ne IX	$1s^2 1S_0 - 1s2p^1 P_1$			11
13.450	13.473	Fe XIX	$2p^4 3P_2 - 2p^3(^2D)3d^3 S_1$	753	.362	20
	13.464	Fe XIX	$2p^4 3P_1 - 2p^3(^2P)3d^3 D_1$			20
	13.521	Fe XIX	$2p^4 3P_2 - 2p^3(^2D)3d^3 D_3$			20, 6
13.517	13.507	Fe XIX	$2p^4 3P_2 - 2p^3(^2D)3d^3 P_2$	1246	.760	20, 6
13.651				383	.129	
13.674	13.671	Fe XIX	$2p^4 3P_1 - 2p^3(^2D)3d^3 P_1$			20, 6
13.701	13.699	Ne IX	$1s^2 1S_0 - 1s2s^3 S_1$	461	.178	7
	13.768	Ni XIX	$2p^6 1S_0 - 2p^5 3s^1 P_1$			6, 23
13.791	13.818	Fe XIX	$2p^4 3P_2 - 2p^3(^4S)3d^3 D_3$	648	.301	20
13.847	13.824	Fe XVII	$2s^2 2p^6 1S_0 - 2s2p^6 3p^1 P_1$			25, 8
13.947				393	.139	
13.967	13.954	Fe XVIII	$2p^5 2P_{3/2} - 2p^4(^1S)3d^2 D_{3/2}$			21
14.025						
14.037	14.043	Ni XIX	$2p^5 1S_0 - 2p^5 3s^3 P_1$	482	.197	16

TABLE 1 (Con't)

SPECTRAL LINES

λ_{obs} Å	$\lambda_{\text{previous}}$ Å	Ion	Transition	Peak Counts (.032s ⁻¹)	Flux (10 ⁶ cm ⁻² s ⁻¹)	Ref.
14.082	14.066	Fe XVIII	$2p^5 2P_{1/2} - 2p^4(^1S)3d^2 D_{3/2}$			24
14.220	14.20	Fe XVIII	$2p^5 2P_{3/2} - 2p^4(^1D)3d^2 D_{5/2}$	1234	.811	21
14.281				654	.324	
14.388	14.373	Fe XVIII	$2p^5 2P_{3/2} - 2p^4(^3P)3d^2 D_{5/2}$	590	.282	22
14.426	14.419	Fe XVIII	$2p^5 2P_{1/2} - 2p^4(^3P)3d^2 F_{5/2}$ $2p^4(^1D)3d^2 P_{3/2}$	415	.166	21
14.477	14.467	Fe XVIII	$2p^5 2P_{1/2} - 2p^4(^1D)3d^2 S_{1/2}$	315	.102	21
14.496	14.485	Fe XVIII	$2p^5 2P_{3/2} - 2p^4(^3P)3d^4 P_{5/2}$			21
14.549	14.551	Fe XVIII	$2p^5 2P_{3/2} - 2p^4(^3P)3d^4 P_{3/2}$	544	.255	21
14.671	14.668	Fe XIX	$2p^4 3P_2 - 2p^3 3s^3 D_3$	406	.165	17
14.743	14.735	Fe XIX	$2p^4 3P_2 - 2p^3 3s^3 D_2$	282	.086	17
14.759	14.754	Fe XVIII	$2p^4 2P_{1/2} - 2p^3(^3P)3d^4 P_{3/2}$			24
14.827	14.821	O VIII	$1s^2 S_{1/2} - 5p^2 P_{1/2, 3/2}$	223	.049	2
14.870				222	.048	
14.919	14.929	Fe XIX	$2p^4 3P_1 - 2p^3 3s^3 D_{2,1}$	292	.095	17
14.962	14.966	Fe XIX	$2p^4 3P_2 - 2p^3 3s^3 S_1$			6
15.013	15.012	Fe XVII	$2p^6 1S_0 - 2p^5 3d^1 P_1$	1663	1.505	25, 8
15.083				589	.318	
15.198	15.176	O VIII	$1s^2 S_{1/2} - 4p^2 P_{1/2, 3/2}$	441	.210	2
	15.172	Fe XIX	$2p^4 3P_1 - 2p^3 3s^3 S_1$			17
15.262	15.260	Fe XVII	$2p^6 1S_0 - 2p^5 3d^3 D_1$	840	.948	25, 8
15.379				212	.047	
15.456	15.453	Fe XVII	$2p^6 1S_0 - 2p^5 3d^3 P_1$	269	.136	25, 8
15.493	15.491	Fe XVIII	$2p^5 2P_{1/2} - 2p^4(^1S)3s^2 S_{1/2}$	193	.082	21
15.511						
15.630	15.623	Fe XVIII	$2p^5 2P_{3/2} - 2p^4(^1D)3s^2 D_{5/2}$	456	.289	6, 22

TABLE 1 (Con't)
SPECTRAL LINES

λ_{obs} Å	$\lambda_{\text{previous}}$ Å	Ion	Transition	Peak Counts (.032s ⁻¹)	Flux (10 ⁶ cm ⁻² s ⁻¹)	Ref.
15.766	15.764	Fe XVIII	$2p^5 2P_{3/2} - 2p^4 (3P) 3s^2 P_{1/2}$	131	.038	21
15.827	15.826	Fe XVIII	$2p^5 2P_{3/2} - 2p^4 (3P) 3s^2 P_{3/2}$	385	.240	22
15.869	15.869	Fe XVIII	$2p^5 2P_{1/2} - 2p^4 (1D) 3s^2 D_{3/2}$	391	.246	21
16.004	16.003	Fe XVIII	$2p^5 2P_{3/2} - 2p^4 (3P) 3s^4 P_{3/2}$	794	.632	22
	16.006	O VIII	$1s^2 S_{1/2} - 3p^2 P_{1/2, 3/2}$			2
16.070	16.073	Fe XVIII	$2p^5 2P_{3/2} - 2p^4 (3P) 3s^4 P_{5/2}$	889	.747	6
16.108	16.109	Fe XVIII	$2p^5 2P_{1/2} - 2p^4 (3P) 3s^4 P_{1/2}$			21
16.165				269	.157	
16.277	16.270	Fe XVIII	$2p^5 2P_{1/2} - 2p^4 (3P) 3s^4 P_{3/2}$	180	.102	21
16.313				200	.119	
16.351				163	.087	
16.775	16.775	Fe XVII	$2p^6 1S_0 - 2p^5 3s^1 P_1$	1058	1.144	25, 8
16.956				150	.088	
17.043	17.051	Fe XVII	$2p^6 1S_0 - 2p^5 3s^3 P_1$	1351	1.715	28, 8
17.084	17.096	Fe XVII	$2p^6 1S_0 - 2p^5 3s^3 P_2$	1293	1.621	28, 8
17.617		Fe	$L\alpha?$	321	.310	
17.76	17.768	O VII	$1s^2 1S_0 - 1s 4p^1 P_1$	104	.062	26
18.625	18.627	O VII	$1s^2 1S_0 - 1s 3p^1 P_1$	130	.159	26
18.969	18.969	O VIII	$1s^2 S_{1/2} - 2p^2 P_{1/2, 3/2}$	874	2.079	2
21.602	21.602	O VII	$1s^2 1S_0 - 1s 2p^1 P_1$	233	.687	26
21.798	21.804	O VII	$1s^2 1S_0 - 1s 2p^3 P_1$	141	.366	26
22.075	22.098	O VII	$1s^2 1S_0 - 1s 2s^3 S_1$	130	.343	29

REFERENCES

- | | |
|---------------------------------------|-------------------------|
| 1. Doschek, Meekins, and Cowan (1972) | 4. Flemberg (1942) |
| 2. Garcia and Mack (1965) | 5. Sawyer et al. (1962) |
| 3. Walker and Rugge (1970, 1971) | 6. Swartz et al. (1971) |

TABLE 1 (Con't)
REFERENCES

-
7. Gabriel and Jordan (1969)
 8. Hutcheon, Pye and Evans (1976)
 9. Neupert et al. (1967), Neupert, Swartz, and Kastner (1973)
 10. Doschek, Meekins, and Cowan (1973)
 11. Peacock, Speer, and Hobby (1969)
 12. Bromage et al. (1977)
 13. Fawcett, Ridgeley, and Hughes (1979)
 14. Bromage, Fawcett, and Cowan (1977)
 15. Breton (1978)
 16. Gordon, Hobby, and Peacock (in prep.)
 17. Bromage et al. (1978)
 18. Bromage and Fawcett (1977b)
 19. Bromage and Fawcett (1977c)
 20. Bromage and Fawcett (1977a)
 21. Feldman et al. (1973)
 22. Fawcett (1965)
 23. Feldman, Cohen, and Swartz (1967)
 24. Boiko et al. (1979)
 25. Tyren (1938)
 26. Tyren (1940)
 27. Fawcett and Hayes (1975)
 28. Parkinson (1973)
 29. Ermolaev and Jones (1973)
 30. Boiko et al. (1977)
-

$$R_M = R \exp (-5.5 \times 10^{-6} R) \quad . \quad (1)$$

The dead time correction was made by solving this equation for R . We then estimated the background counting rate by eye and subtracted it from R (the background required no dead time correction). Finally the resulting counting rate was converted to a line flux by using the spectrometer's peak response as a function of wavelength.

The two main wavelength dependent factors in the response are the detector efficiency and the crystal peak reflectivity. The detector efficiency was determined with the use of laboratory measurements and calculations based upon tabulated x-ray absorption coefficients (Henke and Tester 1975). The only major uncertainty in the relative detector response as a function of wavelength arises from an abrupt change at the fluorine K shell absorption edge at 18.09 Å (the detector has a MgF_2 photocathode). We estimate that the uncertainty in the relative response across this edge is about ten percent. The crystal peak reflectivities were determined from measurements made with a double crystal spectrometer (see McKenzie, Landecker, and Underwood 1976). The integrated reflectivities of the flight crystals were measured, and these agreed very well with the calculations of Burek (1976). These were converted to peak reflectivities under the assumption that the instrumental line shape was Lorentzian. The

resultant peak reflectivities are in excellent agreement with unpublished calculations by Burek (private communication).

In using the peak counting rate as a measure of the incident line flux we considered the following. In the relevant wavelength and plasma temperature ranges, the full width at half maximum (FWHM) of the (approximately Lorentzian) crystal reflectivity curve is 4-8 times the FWHM of the (Gaussian) thermally broadened line. Therefore if the crystal is set at the Bragg angle for a given line, the counting rate (less background) will be, to a very good approximation, equal to the total line flux times the product of the crystal peak reflectivity, the effective area, and the efficiency. Of course, our spectrometer does not sit at the Bragg angle but scans through it and reads out a count accumulation for each one arc minute scan interval. This means the maximum average reflectivity during any accumulation interval is less than the peak reflectivity. Furthermore this maximum average reflectivity varies because the spectrometer cannot sample precisely the same part of the line profile during each scan. We have taken this into account in calculating the effective peak reflectivity and its uncertainty as a function of wavelength. The uncertainty due to this effect varies from less than 1% at about 20 Å to 13% at 8 Å. Doschek, Kreplin, and Feldman (1980) recently measured line broadenings beyond thermal Doppler broadening and attributed them to nonthermal motions with velocities around 100 km/sec. If

such motions were present in the June 10 flare, our effective peak reflectivities are overestimated by about two percent at 8 Å to about ten percent at 20 Å.

For strong unblended lines the uncertainty in the relative fluxes in the table is estimated to be less than 25%. Absolute fluxes are probably accurate to a factor of two. No attempt is made to assign separate background levels to partially blended lines. The fluxes for such lines are therefore overestimated because the background subtracted is underestimated. In a few cases involving severe blends no counting rate or flux is listed for a line, and where two blended lines have about equal counting rates a single rate and flux is assigned to the combination.

Figure 2 shows the time development of the flux in selected lines, emitted in a variety of temperature ranges. The lines selected are the strongest ones available having no known significant blending with lines emitted by other ionic species. The lines and their approximate characteristic temperatures are:

O VII $1s^2 \ ^1S_0 - 1s2p \ ^1P_1$ (21.60 Å), 2×10^6 K; O VIII $1s \ ^2S_{1/2} - 2p \ ^2P_{1/2,3/2}$ (18.97 Å), 3×10^6 K; Mg XII $1s \ ^2S_{1/2} - 2p \ ^2P_{1/2,3/2}$ (8.42 Å), 9×10^6 K; Fe XX $2p^3 \ ^4S_{3/2} - 2p^2(^3P)3d \ ^4P_{5/2,3/2,1/2}$ (12.83 Å), 10×10^6 K; and Fe XXIV $2s \ ^2S_{1/2} - 3p \ ^2P_{3/2}$ (10.64 Å), 17×10^6 K. The flux from each line is normalized to its peak value. While, for the fluxes in Table 1, it was impossible to use integrated line fluxes because of blending, here we are able to

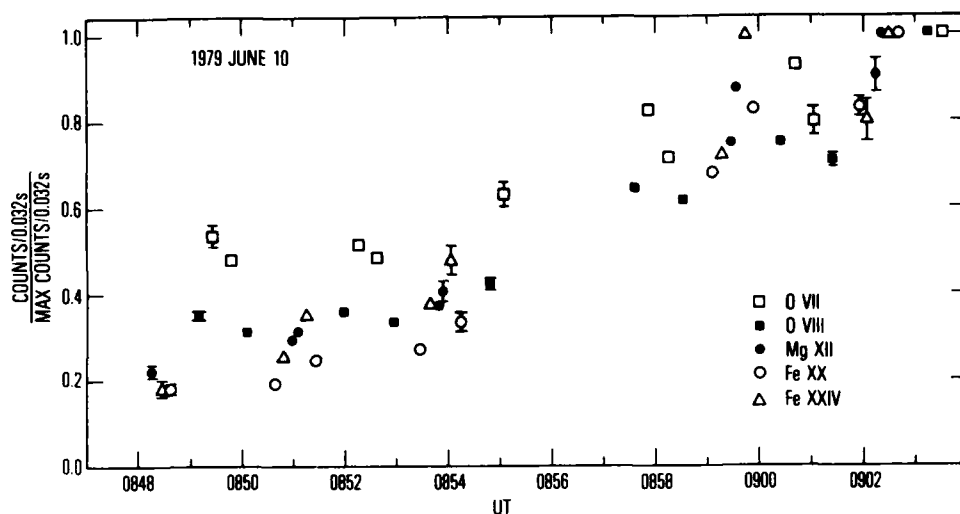


Figure 2: Line flux plotted as a function of time during the rise phase of the 1979 June 10 flare. The flux of each line is normalized to its maximum observed value. The lines are identified in the text.

integrate under the line profile since no comparison is made between different lines. Thus integrated fluxes are used. Again dead time corrections have been applied and background has been subtracted. Selected $\pm 1 \sigma$ error bars are shown. These reflect statistical errors and uncertainties in the background correction.

All of the lines in Figure 2, except the O VII line, are quite similar in their development. The relatively small increase in the O VII emission compared to that of the higher temperature lines could suggest that the flare plasma heated up during the rise phase, but another interpretation is possible. We may be viewing the large burst against a background consisting of the flux from the earlier part of the same flare. When the line fluxes present at 0824 UT are subtracted, as background, from those plotted in Figure 2, all five lines show a similar development. Thus it is quite possible that the flare temperature, or the shape of the curve of emission measure distribution as a function of temperature, underwent little change from just after the start of the rapid rise until the X-ray peak. The similarity in evolution of lines emitted at a wide variety of temperatures prevents us from using these "light curves" to identify the ion species emitting the prominent unidentified lines in Table 1. This analysis awaits the observation of the decay phase of a major flare, when the cooling plasma results in different flux versus time curves for different species.

Table 1 lists over 100 lines. About 75% of these can be identified with confidence, although considerable blending is apparent. The line identifications for elements other than iron and nickel were obtained from Kelly and Palumbo (1973). These lines are apparent in solar active region spectra and have been widely observed previously (e.g., Walker, Rugge and Weiss 1974a, b; Parkinson 1975). The identifications of Fe XVII lines were obtained from Tyén (1938), Parkinson (1973), and Hutcheon, Pye and Evans (1976). These lines are also strong in active region spectra and have been measured by Parkinson (1973), Hutcheon, Pye and Evans (1976), and Walker, Rugge, and Weiss (1974c), and their strengths have been calculated by Louergue and Nussbaumer (1975). The Fe XVIII spectrum has been studied by Rugge and Walker (1978). The lines of Fe XVII and of helium- and hydrogen-like ions of Mg, Ne, and O have been used as standards in establishing the wavelength scale. Their wavelengths are very well known. A survey of other strong, well known, unblended lines in Table 1 yielded an rms deviation between our wavelengths and previously reported values of 14 mÅ.

The lines of Fe XVIII through Fe XXIV and the isoelectronic species of nickel are strong only in flare spectra. The high resolution of the present spectra allows detailed line identifications not possible with earlier flare spectra (e.g., Doschek, Meekins and Cowan 1973; Neupert, Swartz, and Kastner 1973). The

sources for these identifications are given in the table. While many Fe XVIII and Fe XIX lines can be identified, only a few Fe XX lines are present with appreciable intensity. This is because of the low electron densities of solar plasmas (see Bhatia and Mason 1979; Mason et al. 1979).

The identifications of a few lines are uncertain because there are two or more solar lines near the wavelength of a line measured in the laboratory. We have not yet seen enough spectra to be able to clarify these situations by assigning lines to excitation classes. For example, it is not certain which of the two lines at 11.742 and 11.770 Å is due to Fe XXII. We assign the identification to the 11.770 Å line because it is closer in wavelength to the laboratory value of 11.767 Å.

Fe XXI and Fe XXII provide line pairs for density diagnostics useful for temperatures in the range $10-15 \times 10^6$ K. In Fe XXI the ratio $R = I(2p^2 \ ^3P_2 - 2p3d \ ^3D_3)/I(2p^2 \ ^3P_0 - 2p3d \ ^3D_1)$ is sensitive to density in the range $10^{11} - 10^{14} \text{ cm}^{-3}$ (Mason et al. 1979). Bromage and Fawcett (1977b) give wavelengths of 12.38 Å and 12.313 Å for the $^3P_2 - ^3D_3$ and $^3P_0 - ^3D_1$ lines, respectively. We find no strong line at either wavelength, but assign the feature at 12.276 Å to the $^3P_0 - ^3D_1$ line and the line at 12.401 Å to the $^3P_2 - ^3D_3$ transition. Figure 3 is an enlargement of part of the spectrum showing these lines and the Fe XXII lines to be discussed below. The $^3P_0 - ^3D_1$ line is blended with an Fe XVII line. Since

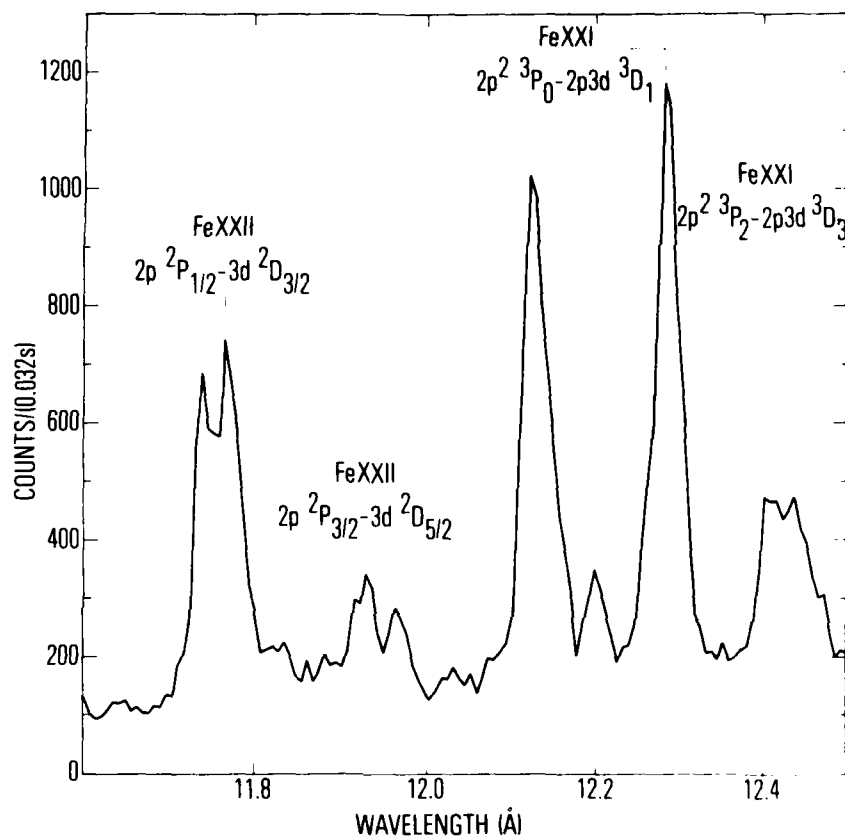


Figure 3: An enlargement of part of the upper spectrum of Figure 1 showing density sensitive Fe XXI and Fe XXII line pairs.

the relative strengths of the Fe XVII lines are not sensitive to density or temperature (Loulergue and Nussbaumer 1975) the Fe XVII contribution to the blend may be determined from, for example, the spectrum of Parkinson (1975). The $^3P_2 - ^3D_3$ line is partially blended with the Ni XIX $2p^6\ ^1S_0 - 2p^53d\ ^1P_1$ line. Unfortunately, our spectrum includes no strong unblended Ni XIX line upon which to base a correction for this blending. We do not attempt here to resolve this blend, but the Fe XXI line ratio should be useful for density diagnostics where unblended Ni XIX measurements exist or the spectral resolution is slightly better than it is for this spectrum.

For Fe XXII the ratio $R' = I(2p\ ^2P_{3/2} - 3d\ ^2D_{5/2})/I(2p\ ^2P_{1/2} - 3d\ ^2D_{3/2})$ is sensitive to density above about 10^{13} cm^{-3} (Mason and Storey 1978). Bromage et al. (1977) have assigned wavelengths of 11.767 Å and 11.921 Å to the $^2P_{1/2} - ^2D_{3/2}$ and $^2P_{3/2} - ^2D_{5/2}$ lines, respectively. Table 1 lists two strong lines near 11.76 Å. We are not sure which is the Fe XXII $^2P_{1/2} - ^2D_{3/2}$ line since both are seen only at high temperature. Fortunately the two lines have about the same intensity, so either can be used. As discussed above, we use the line at 11.770 Å. The 11.92 Å line is blended with the Fe XXII $2p\ ^2P_{3/2} - 3d\ ^2D_{3/2}$ line at 11.937 Å, which is 5.2 times weaker than the 11.92 Å line. Correcting for the $^2P_{3/2} - ^2D_{3/2}$ line we find $R' = 0.20$, which is in the low

density limit and indicates a density below 10^{13} cm^{-3} (Mason and Storey 1978).

The line at 17.62 \AA in Figure 1 is especially interesting. No known line of highly ionized iron exists at this wavelength. The wavelength is in excellent agreement with that of the Fe L α characteristic X-ray. Neupert et al. (1967) and Doschek et al. (1971) have previously observed Fe K α radiation at 1.93 \AA in flares, and Bai (1979) has discussed applications of Fe K α observations. We tentatively identify the line at 17.62 \AA as Fe L α . The line is apparent, but not identified, in spectra reported by Rugge and Walker (1968) and Walker and Rugge (1969). More observations of this line, particularly during the decay phase of flares, are required before a positive identification can be made.

REFERENCES

- Bai, Taeil 1979, Solar Phys., 62, 113.
- Bhatia, A. K. and Mason, H. E., 1979, "New Atomic Data for Fe⁺¹⁹," preprint.
- Boiko, V. A., Pikuz, S. A., Safronova, A. S., and Faenov, A. Ya. 1977, J. Phys. B, 10, 1253.
- Boiko, V. A., Pikuz, S. A., Safronova, A. S., Faenov, A. Ya., Bogdanovich, P. O., Merkelis, G. V., Rudzikas, Z. B., and Sadziuviene, S. D. 1979, J. Phys. B, 12, 1927.
- Breton, C. 1978, Journal de Physique Colloque C4, Suppl., 7, 39, 4.
- Bromage, G. E., Cowan, R. D., Fawcett, B. C., Gordon, H., Hobby, M. G., Peacock, N. J., and Ridgeley, A. 1978, Culham Lab Report CLM-R170 (HMSO).
- Bromage, G. E., Cowan, R. D., Fawcett, B. C., and Ridgeley, A. 1977, J. O. S. A., 68, 48.
- Bromage, G. E., and Fawcett, B. C. 1977a, M. N. R. A. S., 178, 591.
- Bromage, G. E., and Fawcett, B. C. 1977b, M. N. R. A. S., 178, 605.
- Bromage, G. E., and Fawcett, B. C. 1977c, M. N. R. A. S., 179, 683.

- Bromage, G. E., Fawcett, B. C., and Cowan, R. D. 1977, M. N. R. A. S., 178, 599.
- Burek, Anthony 1976, Space Sci. Inst., 2, 53.
- Doschek, G. A., Kreplin, R. W., and Feldman, U. 1980, Ap. J. (Letters), 233, L157.
- Doschek, G. A., Meekins, J. F., and Cowan, R. D. 1972, Ap. J., 177, 261.
- Doschek, G. A., Meekins, J. F., and Cowan, R. D. 1973, Solar Phys., 29, 125.
- Doschek, G. A., Meekins, J. F., Kreplin, R. W., Chubb, T. A., and Friedman, H. 1971, Ap. J., 170, 573.
- Ermolaev, A. M. and Jones, M. 1973, British National Reference Library, Ref. No. SUP 70009.
- Fawcett, B. C. 1965, Proc. Phys. Soc. Lond., 86, 1087.
- Fawcett, B. C., and Hayes, R. W. 1975, M. N. R. A. S., 170, 185.
- Fawcett, B. C., Ridgeley, A., and Hughes, T. P. 1979, M. N. R. A. S., 188, 365.
- Feldman, U., Cohen, L. and Swartz M. 1967, Ap. J., 148, 585.
- Feldman, U., Doschek, G. A., Cowan, R. D., and Cohen, L., 1973, J. O. S. A., 63, 1445.
- Flemberg, H. 1942, Ark. Mat. Astron. Fysik, 28A, No. 18, 1.
- Gabriel, A. H., and Jordan, C. 1969, Nature, 221, 947.
- Garcia, J. D., and Mack, J. E. 1965, J.O.S.A., 55, 654.
- Gordon, H., Hobby, M. G., and Peacock, N. J. 1980, (in prep).

- Henke, B. L. and Tester, M. A. 1975, Advances in X-ray Analysis,
18, 76.
- Hutcheon, R. J., Pye, J. P., and Evans, K. D., 1976, Astr. Ap. 51,
451.
- Kelly, Raymond L., and Palumbo, Louis J. 1973, "Atomic and Ionic
Emission Lines below 2000 Angstroms Hydrogen through Krypton"
U. S. Gov. Printing Office.
- Landecker, P. B., McKenzie, D. L., and Rugge, H. R. 1979, Proc.
SPIE, 184, 285.
- Loulergue, M. and Nussbaumer, H. 1975, Astr. Ap., 45, 125.
- Mason, H. E., Doschek, G. A., Feldman, U., and Bhatia, A. K. 1979,
Astr. Ap., 73, 74.
- Mason, H. E., and Storey, P. J. 1978, "Atomic Data for Fe XXII,"
preprint.
- McKenzie, D. L., Landecker, P. B., and Underwood, J. H. 1976,
Space Sci. Inst., 2, 125.
- Neupert, W. M., Gates, W., Swartz, M., and Young, R. M. 1967, Ap.
J. (Letters), 149, L79.
- Neupert, W. M., Swartz, M., and Kastner, S. O. 1973, Solar Phys.,
31, 171.
- Parkinson, J. H. 1973, Astr. Ap., 24, 215.
- Parkinson, J. H. 1975, Solar Phys., 42, 183.
- Peacock, N. J., Speer, R. J., and Hobby, M. G. 1969, J. Phys. B,
2, 798.

- Rugge, H. R., and Walker, A. B. C., Jr. 1968, Space Research, 8, 439.
- Rugge, H. R., and Walker, A. B. C., Jr. 1978, Ap. J., 219, 1068.
- Sawyer, G. A., Jahoda, F. C., Kibe, F. L., and Stratton, T. F., 1962, J.Q.S.R.T., 2, 467.
- Solar Geophysical Data, 419 Part 1, p 18, July 1979, U. S. Dept. of Commerce (Boulder, Colorado, U. S. A., 80303).
- Swartz, M., Kastner, S., Rothe, E., and Neupert, W. 1971, J. Phys. B, 4, 1747.
- Tyrén, F. 1938, Z. Physik, 111, 314.
- Tyrén, F. 1940, Nova Acta Reg. Soc. Sci. Upsala, 12, No. 1, 7.
- Walker, A. B. C., Jr., and Rugge, H. R. 1969, Solar Flares and Space Research (North Holland, Amsterdam), 102.
- Walker, A. B. C., Jr., and Rugge, H. R. 1970, Astr. Ap., 5, 4.
- Walker, A. B. C., Jr., and Rugge, H. R. 1971, Ap. J., 164, 181.
- Walker, A. B. C., Jr., Rugge, H. R., and Weiss, K. 1974a, Ap. J., 188, 423.
- Walker, A. B. C., Jr., Rugge, H. R., and Weiss, K. 1974b, Ap. J., 192, 169.
- Walker, A. B. C., Jr., Rugge, H. R., and Weiss, K. 1974c, Ap. J., 194, 471.

LABORATORY OPERATIONS

The Laboratory Operations of The Aerospace Corporation is conducting experimental and theoretical investigations necessary for the evaluation and application of scientific advances to new military concepts and systems. Versatility and flexibility have been developed to a high degree by the laboratory personnel in dealing with the many problems encountered in the Nation's rapidly developing space systems. Expertise in the latest scientific developments is vital to the accomplishment of tasks related to these problems. The laboratories that contribute to this research are:

Aerophysics Laboratory: Aerodynamics; fluid dynamics; plasmadynamics; chemical kinetics; engineering mechanics; flight dynamics; heat transfer; high-power gas lasers, continuous and pulsed, IR, visible, UV; laser physics; laser resonator optics; laser effects and countermeasures.

Chemistry and Physics Laboratory: Atmospheric reactions and optical backgrounds; radiative transfer and atmospheric transmission; thermal and state-specific reaction rates in rocket plumes; chemical thermodynamics and propulsion chemistry; laser isotope separation; chemistry and physics of particles; space environmental and contamination effects on spacecraft materials; lubrication; surface chemistry of insulators and conductors; cathode materials; sensor materials and sensor optics; applied laser spectroscopy; atomic frequency standards; pollution and toxic materials monitoring.

Electronics Research Laboratory: Electromagnetic theory and propagation phenomena; microwave and semiconductor devices and integrated circuits; quantum electronics, lasers, and electro-optics; communication sciences, applied electronics, superconducting and electronic device physics; millimeter-wave and far-infrared technology.

Materials Sciences Laboratory: Development of new materials; composite materials; graphite and ceramics; polymeric materials; weapons effects and hardened materials; materials for electronic devices; dimensionally stable materials; chemical and structural analyses; stress corrosion; fatigue of metals.

Space Sciences Laboratory: Atmospheric and ionospheric physics, radiation from the atmosphere, density and composition of the atmosphere, aurorae and airglow; magnetospheric physics, cosmic rays, generation and propagation of plasma waves in the magnetosphere; solar physics, x-ray astronomy; the effects of nuclear explosions, magnetic storms, and solar activity on the earth's atmosphere, ionosphere, and magnetosphere; the effects of optical, electromagnetic, and particulate radiations in space on space systems.

. . .